Superconducting Gap Anisotropy in Monolayer FeSe Thin Film

Y. Zhang,[1,2] J. J. Lee,[1,3] R. G. Moore,[1] W. Li,[1] M. Yi,[1,3] M. Hashimoto,[4] D. H. Lu,[4] T. P. Devereaux,[1,3] D.-H. Lee,[5,6] and Z.-X. Shen[1,3,*]

[1]*Stanford Institute for Materials and Energy Sciences, SLAC National Accelerator Laboratory, 2575 Sand Hill Road, Menlo Park, California 94025, USA*

[2]*Advanced Light Source, Lawrence Berkeley National Laboratory, Berkeley, California 94720, USA*

[3]*Geballe Laboratory for Advanced Materials, Departments of Physics and Applied Physics, Stanford University, Stanford, California 94305, USA*

[4]*Stanford Synchrotron Radiation Lightsource, SLAC National Accelerator Laboratory, 2575 Sand Hill Road, Menlo Park, California 94025, USA*

[5]*Department of Physics, University of California at Berkeley, Berkeley, California 94720, USA*

[6]*Material Science Division, Lawrence Berkeley National Laboratory, Berkeley, California 94720, USA*

(Received 9 March 2016; published 8 September 2016)

Superconductivity originates from pairing of electrons near the Fermi energy. The Fermi surface topology and pairing symmetry are thus two pivotal characteristics of a superconductor. Superconductivity in one monolayer (1 ML) FeSe thin film has attracted great interest recently due to its intriguing interfacial properties and possibly high superconducting transition temperature over 65 K. Here, we report high-resolution measurements of the Fermi surface and superconducting gaps in 1 ML FeSe using angle-resolved photoemission spectroscopy. Two ellipselike electron pockets are clearly resolved overlapping with each other at the Brillouin zone corner. The superconducting gap is nodeless but moderately anisotropic, which puts strong constraint on determining the pairing symmetry. The gap maxima locate on the d_{xy} bands along the major axis of the ellipse and four gap minima are observed at the intersections of electron pockets. The gap maximum location combined with the Fermi surface geometry deviate from a single d-wave, extended s-wave or $s_{\pm}$ gap function, suggesting an important role of the multiorbital nature of Fermi surface and orbital-dependent pairing in 1 ML FeSe. The gap minima location may be explained by a sign change on the electron pockets, or a competition between intra- and interorbital pairing.

DOI: 10.1103/PhysRevLett.117.117001

The discovery of superconductivity in monolayer (1 ML) FeSe thin film has generated great interest [1–12]. The superconducting gap closing temperature was reported to be over 65 K, which holds the record in iron-based superconductors. More intriguingly, angle-resolved photoemission spectroscopy (ARPES) studies showed that the Fermi surface consists only of electron pockets at the corner of the Brillouin zone and there are no hole pockets at the zone center as typically found in iron-based superconductors [2–4,10]. Based on such a Fermi surface topology, several pairing symmetries have been proposed theoretically [13–19]: d-wave and extended s-wave pairing symmetries, where the gaps change sign between different parts of the Fermi surface; s-wave and $s_{\pm}$ pairing symmetries, where there is no sign change on the Fermi surface. In early studies, the superconducting gaps were found to be nearly isotropic on the electron pockets [2,4]; however, they provide insufficient information to address the critical issue of pairing symmetry in 1 ML FeSe.

Here, we study the 1 ML FeSe film using high-resolution ARPES. By choosing different light polarization, two ellipselike electron pockets are clearly resolved and the superconducting gap distribution on the electron pockets is measured with high precision. We found that the superconducting gap is nodeless but moderately anisotropic on the electron pockets. The gap maxima locate along the major axis of ellipse where the bands are constructed by the d_{xy} orbital and four gap minima are observed at the intersections of two ellipselike electron pockets. The location of the gap maxima cannot be fitted by a single trigonometric gap function under d-wave, extended s-wave, or $s_{\pm}$ pairing symmetry, which suggests that the multiorbital nature of Fermi surface and orbital-dependent pairing are important for superconducting pairing. The location of gap minima can be explained by either a sign change on the electron pockets, or a competition between intra- and interorbital pairing in 1 ML FeSe.

FeSe films were grown on high quality Nb-doped (0.05 wt. %) $SrTiO_3$ (100) substrates. TiO_2 terminated atomic flat surface were prepared by degassing at 450 °C for several hours and subsequently annealing at 900 °C for 20 min. Ultrahigh purity selenium (99.999%) was evaporated from an effusion cell with a thermal cracking insert (Createc) while iron (99.995%) was evaporated from a 2 mm rod using an electron beam evaporator (Specs). The growth was carried out under Se-rich condition with a Se/Fe flux ratio of 3–4. Substrate temperatures were kept at 380 °C during the growth. The films were subsequently

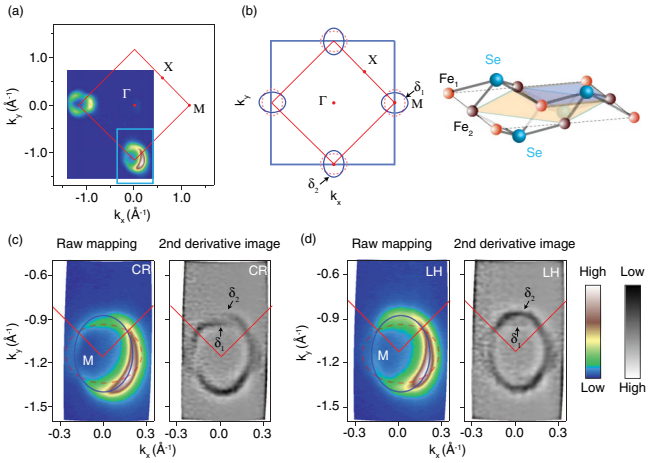

FIG. 1. Fermi surface topology. (a) Fermi surface mapping of 1 ML FeSe taken in circular (CR) polarization. The Brillouin zone is defined by the two-iron unit cell with the Γ-M direction along the iron-iron bond direction. (b) The one- and two-iron unit cells in the iron-pnictogen/chalcogen plane (right panel) and the corresponding one- and two-iron Brillouin zones and Fermi surfaces (left panel). (c) Fermi surface mapping (left panel) and its second derivative image (right panel) taken in CR polarization at ∼120 K using high energy and momentum resolution. The derivation was taken along both k_x and k_y direction. (d) is the same as (c), but taken with linear horizontal (LH) polarization. The in-plane polarization vector is along the k_x direction.

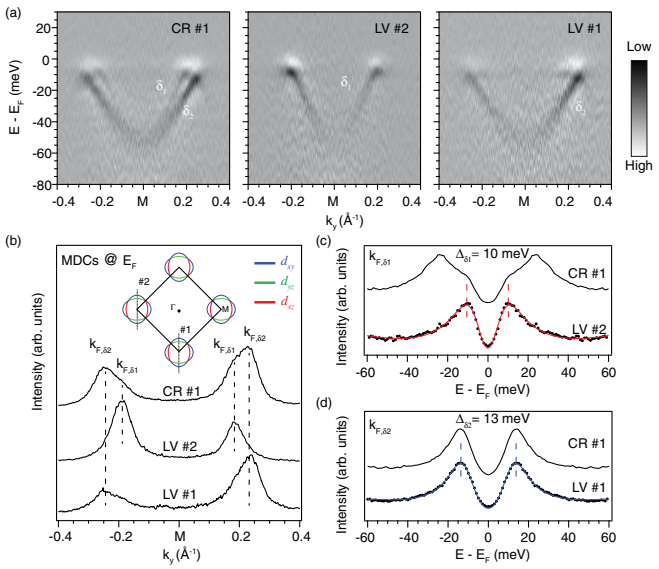

FIG. 2. Multigap behavior of the superconducting state. (a) The second derivative images of photoemission spectra taken in CR and linear vertical (LV) polarization at 20 K. The in-plane polarization vector is along the k_y direction for LV polarization. The momenta of cut no. 1 and cut no. 2 are shown in the inset of (b). (b) The corresponding MDCs taken at the Fermi energy (E_F) of the data in (a). The inset of (b) shows the orbital character of Fermi surface. (c) Symmetrized EDCs taken at the Fermi crossings (k'_F s) of the δ_1 electron band with CR and LV polarization. The gap magnitude was obtained by fitting the symmetrized EDCs (black dots) using a phenomenological superconducting spectra function [28]. The fitting result is shown by the red solid line. (d) is the same as (c) but taken at the k'_F s of the δ_2 electron band.

annealed at 450 °C for four hours immediately after growth. The T_C of the film is around 55 K as determined by the gap closing temperature [10]. The films were transported to the ARPES chamber via a vacuum suitcase with base pressure of 5×10^{-10} torr. ARPES measurements were performed at the Stanford Synchrotron Radiation Lightsource Beamline 5-4. The data were taken with 22 eV photons. The temperature was kept at 20 K for the superconducting gap measurement. The overall energy resolution was 5 meV, and the angular resolution was less than 0.3°. All the samples were measured in ultrahigh vacuum with a base pressure better than 3×10^{-11} torr.

Clear delineation of the Fermi surface is important for determining the gap structure in 1 ML FeSe. As shown in Fig. 1(a), the ARPES intensity map shows one circularlike Fermi surface at M and no Fermi surface at the zone center (Γ). This result is consistent with previous studies [2–4,10]. However, by performing high-resolution measurements at the M point using particular photon polarizations, two ellipselike electron pockets are clearly resolved [Figs. 1(c) and 1(d)]. According to the band calculations, the Fermi surface consists of one ellipse electron pocket at each Brillouin zone boundary in one-iron Brillouin zone [20,21] [Fig. 1(b)]. When the glide-mirror symmetry of the iron-selenium plane is considered, the unit cell doubles and the Brillouin zone folds [22]. As a result, the horizontal ellipse pocket (δ_1) folds onto the vertical ellipse pocket (δ_2) in the two-iron Brillouin zone [Fig. 1(b)]. This is consistent with the observed Fermi surface topology at the M point [Figs. 1(c) and 1(d)]. The photoemission intensity of the main band δ_2, is much higher than that of the folded band δ_1 at the bottom corner of the two-iron Brillouin zone. A similar ellipselike shape of electron pockets has also been observed in 1 ML FeSe grown on strained $SrTiO_3$ [23].

According to the band calculations, either the spin-orbital coupling or the breaking of glide-mirror symmetry would lift the band degeneracy at the Fermi surface crossing of two ellipses in two-iron Brillouin zone [24,25]. For 1 ML FeSe film grown on $SrTiO_3$, finite spin-orbital coupling is present as observed in bulk FeSe [26] and the glide-mirror symmetry no longer exists due to the presence of substrate. Therefore, it is expected that there is finite hybridization between the δ_1 and δ_2 ellipse electron pockets. However, no avoided crossings are observed at the intersections of two electron pockets, indicating that the hybridization caused by either the spin-orbit interaction or the lack of glide-mirror symmetry is too small to be observed under our experimental resolution (∼5 meV).

Figure 2 shows the superconducting gaps associated with the δ_1 and δ_2 electron bands along the Γ-M direction. Two electron bands are clearly resolved in the second derivative

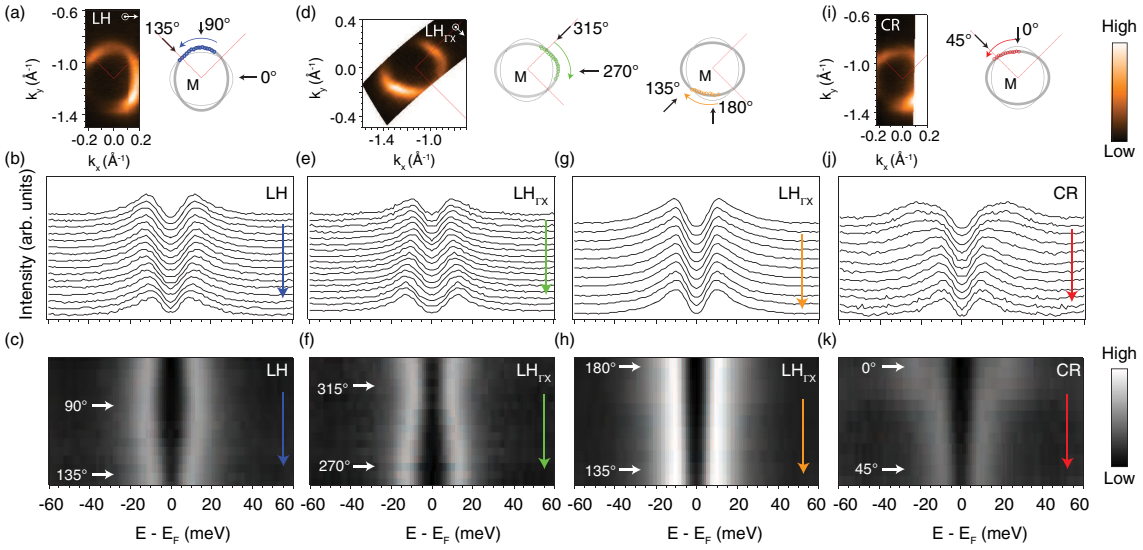

FIG. 3. Momentum dependence of the superconducting gaps on the electron pockets. (a) The Fermi surface mapping taken in LH polarization. The polarization vector is shown in the inset. (b) Symmetrized EDCs taken on one section of the electron pockets. The momenta of the data points are shown in (a). (c) Merged image of the symmetrized EDCs in (a), which highlights the variation of the superconducting peak positions. (d)–(k) are the same as (a) and (c), but taken on different sections of the electron pockets.

images along the M-Γ direction [Fig. 2(a)]. By using linear vertical polarization (LV), the δ_1 and δ_2 bands can be probed selectively by choosing the cut momenta at either the left or bottom corner of the Brillouin zone [Fig. 2(b)]. If we define a mirror plane by the sample normal and cut in the no. 1 direction, the LV polarization is even with respect to the mirror plane. According to the symmetry argument of the photoemission process [22,27], the δ_2 band exhibits even symmetry suggesting its d_{xy} orbital character. The δ_1 band was then attributed to the d_{xz}/d_{yz} orbitals according to the band calculations. The orbital character of the Fermi surface is shown in the inset of Fig. 2(b). The orbital selectivity of different polarizations enables us to probe different bands separately, which is crucial for measuring the superconducting gaps in a multiband system. The back bendings of bands are clearly observed attesting for the high data quality. The gap magnitude is determined by the gap fitting of symmetrized EDCs at the relevant k'_F s [Figs. 2(c) and 2(d)], i.e., the gap minima of the corresponding band dispersions [Fig. 2(a)]. The superconducting gap is ~10 meV for the δ_1 band and ~13 meV for the δ_2 band.

The multigap behavior on δ_1 and δ_2 suggests that the superconducting gap is anisotropic. By choosing a different experimental setup, we can selectively measure the superconducting gap on different sections of the electron pockets (Fig. 3). The gap anisotropy is obvious near the major axis of the ellipses [Figs. 3(a)–3(f)], and manifested by the maxima along the 90° and 270° directions in Figs. 3(c) and 3(f), respectively.

Because no hybridization is observed between two ellipses, we could then map the gap measurement data onto one ellipse electron pocket. The results are shown in Figs. 4(a)–4(b). The smooth evolution of the gap tied to the underlying Fermi surface is consistent with it being a superconducting gap. Because ARPES measures the absolute value of the gap function we perform a best fit of the observed energy gap as a function of angle around the Fermi pocket by $|f(\theta)|$. The result of such fitting gives $f(\theta) = (9.98 \pm 0.10) - (1.24 \pm 0.13)\cos 2\theta + (1.15 \pm 0.13)\cos 4\theta$ meV.

One characteristic of the gap anisotropy is that the gap maxima locate along the major axis of the ellipse (the 90° and 270° directions). We simulated the gap distribution on the δ_2 electron pocket using several trigonometric gap functions that are proposed under d-wave, $s_\pm$ and extended s-wave pairing symmetries [Figs. 4(d)–4(f)]. For the $|(\cos k_x - \cos k_y)/2|$ and $|\cos k_x \cos k_y|$ gap functions, the pair strength is strongest at the center of the ellipse electron pockets meaning that the gap maxima should locate along the minor axis of the ellipse (0° and 180° directions) [Figs. 4(e) and 4(f)]. This contradicts our observation. For the $|(\cos k_x + \cos k_y)/2|$ gap function, it generates gap maxima along the correct directions. However, the $|(\cos k_x + \cos k_y)/2|$ gap function is not energy favored in 1 ML FeSe because the pairing strength is strongest at the center and corner of the one-iron Brillouin zone where there is no Fermi surface. In order to achieve the 8–13 meV gap magnitude on the electron pockets, a large and unrealistic gap value (> 100 meV) needs to be used in the simulation. Therefore, the observed momentum locations of the gap maxima cannot be explained by a single trigonometric gap function.

The origin of gap anisotropy is still being debated for iron-based superconductors. In $Ba_{1-x}K_xFe_2As_2$, the gap anisotropy was explained by $s_\pm$-wave gap function [29], while in LiFeAs, the gap anisotropy was attributed to

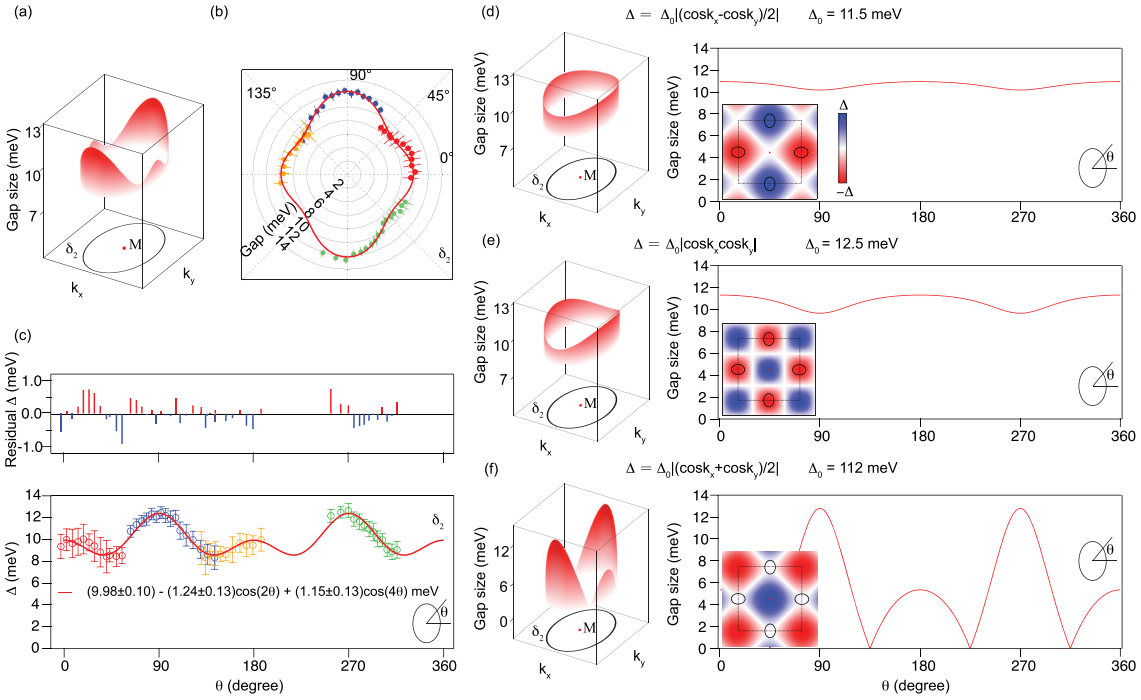

FIG. 4. Superconducting gap anisotropy in 1 ML FeSe. (a) and (b) Superconducting gap anisotropy on the ellipselike electron pocket δ_2. The gap magnitudes were obtained by fitting the symmetrized EDCs in Fig. 3 using a phenomenological superconducting spectral function [28]. The gap measurement data were mapped onto δ_2 ellipse pocket according to the $C4$ rotational symmetry. The error bars are estimated by the fitting process. (c) Phenomenology function fitting of the gap anisotropy in 1 ML FeSe. The residual values are shown in the upper panel presenting the fitting quality. The fitting result is shown by the red solid line with the function $(9.98 \pm 0.10) - (1.24 \pm 0.13)\cos 2\theta + (1.15 \pm 0.13)\cos 4\theta$ meV. (d), Simulation of the gap anisotropy on the δ_2 electron pocket using the $|(\cos k_x - \cos k_y)/2|$ gap function. The inset panel illustrates the sign change on the Fermi surface. (e) and (f) are the same as (d) but calculated using $|\cos k_x \cos k_y|$ and $|(\cos k_x + \cos k_y)/2|$ gap functions.

either a $s_{\pm}$-wave gap function or an orbital-fluctuation meditated pairing [30,31]. Here in 1 ML FeSe, the clear deviation from single trigonometric gap function implicates the importance of a multiorbital Fermi surface and orbital-dependent pairing [14,19]. The gap maxima locate on the d_{xy} bands suggesting the dominating role of d_{xy} intraorbital pairing in 1 ML FeSe. This contradicts to what has been observed in iron pnictides where the d_{xz}/d_{yz} bands are proposed to play a more important role in superconducting pairing and the gap minima or gap nodes locate on the d_{xy} bands [13,29,32]. One possible explanation is the orbital-selective correlation observed in iron chalcogenides [33]. The d_{xy} orbital is much more correlated than the d_{xz}/d_{yz} orbitals, hence showing a larger superconducting gap.

Another characteristic of the gap anisotropy is the presence of four gap minima along the 45° directions of the ellipse. On one hand, the gap minima can be viewed as an indication for the existence of sign change on the electron pockets. If the gap changes sign near the intersection of δ_1 and δ_2, such as the gap under d-wave and extended s-wave pairing symmetries, the hybridization between δ_1 and δ_2 would mix the gaps with opposite sign and generate gap minima or gap nodes depending on the strength of the hybridization [13,15]. On the other hand, the gap minima may originate from the competition between intraorbital and interorbital pairing under s-wave pairing symmetry [19]. The electron pockets are constructed by d_{xz}/d_{yz} and d_{xy} orbitals and the orbital character varies when moving around the Fermi surface [20–22,27]. The gap minima locate along the 45° directions of the ellipses where the mixing of d_{xz}/d_{yz} and d_{xy} orbitals is strongest. The gap would be minima if the intraorbital pairing dominates the pairing interaction in 1 ML FeSe.

In summary, we conducted high-resolution measurements of the Fermi surface and superconducting gaps in 1 ML FeSe. Two ellipselike electron pockets are resolved overlapping with each other at the zone corner. The superconducting gap distribution on the electron pockets shows distinct anisotropy. The gap maxima locate along the major axis of he ellipse, suggesting the importance of multiorbital physics in 1 ML FeSe. Four gap minima locate at the intersection of two ellipselike electron pockets, which can be explained by a sign change on electron pockets, or a competition between intra- and interorbital pairing. Our results put strong constraints on determining the pairing symmetry and provide a starting point for further quantitative theoretical analyses.

ARPES experiments were performed at the Stanford Synchrotron Radiation Lightsource, which is operated by the Office of Basic Energy Sciences, U.S. Department of Energy. The Stanford work is supported by the U.S. DOE, Office of Basic Energy Science, Division of Materials Science and Engineering. D.-H. L. was supported by the U.S. Department of Energy, Office of Science, Basic Energy Sciences, Materials Sciences and Engineering Division, Grant No. DE-AC02-05CH11231.

*zxshen@stanford.edu

[1] W. Qing-Yan, L. Zhi, Z. Wen-Hao, Z. Zuo-Cheng, Z. Jin-Song, L. Wei, D. Hao, O. Yun-Bo, D. Peng, C. Kai, W. Jing, S. Can-Li, H. Ke, J. Jin-Feng, J. Shuai-Hua, W. Ya-Yu, W. Li-Li, C. Xi, M. Xu-Cun, and X. Qi-Kun, Chin. Phys. Lett. **29**, 037402 (2012).
[2] D. Liu *et al.*, Nat. Commun. **3**, 931 (2012).
[3] S. He *et al.*, Nat. Mater. **12**, 605 (2013).
[4] S. Tan, Y. Zhang, M. Xia, Z. Ye, F. Chen, X. Xie, R. Peng, D. Xu, Q. Fan, H. Xu, J. Jiang, T. Zhang, X. Lai, T. Xiang, J. Hu, B. Xie, and D. Feng, Nat. Mater. **12**, 634 (2013).
[5] Z. Wen-Hao *et al.*, Chin. Phys. Lett. **31**, 017401 (2014).
[6] R. Peng, H. C. Xu, S. Y. Tan, H. Y. Cao, M. Xia, X. P. Shen, Z. C. Huang, C. H. P. Wen, Q. Song, T. Zhang, B. P. Xie, X. G. Gong, and D. L. Feng, Nat. Commun. **5**, 5044 (2014).
[7] L. Z. Deng, B. Lv, Z. Wu, Y. Y. Xue, W. H. Zhang, F. S. Li, L. L. Wang, X. C. Ma, Q. K. Xue, and C. W. Chu, Phys. Rev. B **90**, 214513 (2014).
[8] J.-F. Ge, Z.-L. Liu, C. Liu, C.-L. Gao, D. Qian, Q.-K. Xue, Y. Liu, and J.-F. Jia, Nat. Mater. **14**, 285 (2015).
[9] Y.-Y. Xiang, F. Wang, D. Wang, Q.-H. Wang, and D.-H. Lee, Phys. Rev. B **86**, 134508 (2012).
[10] J. J. Lee, F. T. Schmitt, R. G. Moore, S. Johnston, Y.-T. Cui, W. Li, M. Yi, Z. K. Liu, M. Hashimoto, Y. Zhang, D. H. Lu, T. P. Devereaux, D.-H. Lee, and Z.-X. Shen, Nature (London) **515**, 245 (2014).
[11] S. Coh, M. L. Cohen, and S. G. Louie, New J. Phys. **17**, 073027 (2015).
[12] T. Bazhirov and M. L Cohen, J. Phys. Condens. Matter **25**, 105506 (2013).
[13] P. J. Hirschfeld, M. M. Korshunov, and I. I. Mazin, Rep. Prog. Phys. **74**, 124508 (2011).
[14] T. A. Maier, S. Graser, P. J. Hirschfeld, and D. J. Scalapino, Phys. Rev. B **83**, 100515 (2011).
[15] I. I. Mazin, Phys. Rev. B **84**, 024529 (2011).
[16] N. Hao and J. Hu, Phys. Rev. B **89**, 045144 (2014).
[17] F. Yang, F. Wang, and D.-H. Lee, Phys. Rev. B **88**, 100504 (2013).
[18] T. Saito, S. Onari, and H. Kontani, Phys. Rev. B **83**, 140512 (2011).
[19] C.-H. Lin, C.-P. Chou, W.-G. Yin, and W. Ku, arXiv: 1403.3687.
[20] K. Kuroki, S. Onari, R. Arita, H. Usui, Y. Tanaka, H. Kontani, and H. Aoki, Phys. Rev. Lett. **101**, 087004 (2008).
[21] S. Graser, T. A. Maier, P. J. Hirschfeld, and D. J. Scalapino, New J. Phys. **11**, 025016 (2009).
[22] V. Brouet, M. F. Jensen, P.-H. Lin, A. Taleb-Ibrahimi, P. Le Fèvre, F. Bertran, C.-H. Lin, W. Ku, A. Forget, and D. Colson, Phys. Rev. B **86**, 075123 (2012).
[23] R. Peng, X. P. Shen, X. Xie, H. C. Xu, S. Y. Tan, M. Xia, T. Zhang, H. Y. Cao, X. G. Gong, J. P. Hu, B. P. Xie, and D. L. Feng, Phys. Rev. Lett. **112**, 107001 (2014).
[24] S. V. Borisenko, D. V. Evtushinsky, Z.-H. Liu, I. Morozov, R. Kappenberger, S. Wurmehl, B. Büchner, A. N. Yaresko, T. K. Kim, M. Hoesch, T. Wolf, and N. D. Zhigadlo, Nat. Phys. **12**, 311 (2016).
[25] C.-H. Lin, T. Berlijn, L. Wang, C.-C. Lee, W.-G. Yin, and W. Ku, Phys. Rev. Lett. **107**, 257001 (2011).
[26] P. Zhang, T. Qian, P. Richard, X. P. Wang, H. Miao, B. Q. Lv, B. B. Fu, T. Wolf, C. Meingast, X. X. Wu, Z. Q. Wang, J. P. Hu, and H. Ding, Phys. Rev. B **91**, 214503 (2015).
[27] Y. Zhang, F. Chen, C. He, B. Zhou, B. P. Xie, C. Fang, W. F. Tsai, X. H. Chen, H. Hayashi, J. Jiang, H. Iwasawa, K. Shimada, H. Namatame, M. Taniguchi, J. P. Hu, and D. L. Feng, Phys. Rev. B **83**, 054510 (2011).
[28] M. R. Norman, M. Randeria, H. Ding, and J. C. Campuzano, Phys. Rev. B **57**, R11093 (1998).
[29] D. V. Evtushinsky, V. B. Zabolotnyy, T. K. Kim, A. A. Kordyuk, A. N. Yaresko, J. Maletz, S. Aswartham, S. Wurmehl, A. V. Boris, D. L. Sun, C. T. Lin, B. Shen, H. H. Wen, A. Varykhalov, R. Follath, B. Büchner, and S. V. Borisenko, Phys. Rev. B **89**, 064514 (2014).
[30] S. V. Borisenko, V. B. Zabolotnyy, A. A. Kordyuk, D. V. Evtushinsky, T. K. Kim, I. V. Morozov, R. Follath, and B. Büchner, Symmetry **4**, 251 (2012).
[31] K. Umezawa, Y. Li, H. Miao, K. Nakayama, Z.-H. Liu, P. Richard, T. Sato, J. B. He, D.-M. Wang, G. F. Chen, H. Ding, T. Takahashi, and S.-C. Wang, Phys. Rev. Lett. **108**, 037002 (2012).
[32] A. F. Kemper, T. A. Maier, S. Graser, H.-P. Cheng, P. J. Hirschfeld, and D. J. Scalapino, New J. Phys. **12**, 073030 (2010).
[33] M. Yi *et al.*, Nat. Commun. **6**, 7777 (2015).